A Record of Water-Ice Cloud at the Phoenix Landing Site Derived from Modelling MET Temperature Data

G. Bischof[1], **J.E. Moores**[1], **H.M. Sapers**[1], *Centre for Research in Earth and Space Science, York University, Toronto, Canada (gbischof@yorku.ca)*[1], **B.A. Cooper**[2], *NOIRlab, Gemini North Observatory, Hilo, USA*[2]

Introduction:

The Phoenix mission played a key role in our current understanding of polar clouds. Previous studies have investigated the opacity (Dickinson et al., 2010), morphology (Moores et al., 2010), and transport (Whiteway et al., 2009) of the water-ice clouds throughout the 151-sol mission in the Martian northern polar region (68.2°N).

The lidar and Surface Stereo Imager (SSI) onboard the Phoenix lander were the two main instruments used for characterization of the clouds. However, both instruments leave large temporal gaps in the coverage of clouds. The lidar was used only a few times per sol, with no overnight coverage at the beginning and end of the mission. Similarly, atmospheric movies captured with the SSI encompass only 0.76% of the length of the entire mission (Moores et al., 2010).

The Meteorological (MET) station onboard the Phoenix lander, however, ran near-continuously throughout the mission, taking measurements of the air temperature at 2 m, 1.5 m, and 1 m above the surface every 2 seconds. Investigations into water-ice clouds in other regions of Mars show that the absorption and emission of longwave flux by clouds can influence the surface and near-surface atmospheric temperature, particularly in the nighttime (Wilson et al., 2007; Cooper et al., 2021).

We can exploit the near-continuous coverage of the MET instrument to model a record of clouds throughout the Phoenix mission by isolating cloud emission from the surface energy balance. We compare the cloud emission with water-ice optical depths retrieved from the lidar (Dickson et al. 2010) to provide a unique examination of the radiative properties of Martian water-ice clouds.

Methods:

MET Suite on Phoenix. The MET instrument suite onboard the Phoenix lander carried three fine-wire thermocouple temperature sensors, located 1 m, 1.5 m, and 2 m from the surface, with a measurement frequency of 0.5 Hz. The temperature sensors had an uncertainty of ± 1 K (Taylor et al., 2008). A pressure sensor took measurements of the atmospheric pressure at 2 m at the same cadence as the temperature measurement. A tell-tale wind-indicator was included to monitor the direction and speed of the wind.

Reduced Data Records (RDRs) form each sol were acquired for this work from the Planetary Data System: Atmospheres Node. We use the data from the 2 m air temperature sensor to avoid any heat contamination given off from the lander.

Surface Energy Balance and Cloud Emission. This work seeks to build a record of clouds at the Phoenix site by analyzing the radiative contribution of the water-ice clouds to the surface energy balance. The energy balance used in this work is adapted from Martínez et al. (2014) and is given by

$$G = S(1-\alpha) + LW_{\downarrow} - LW_{\uparrow} - H - LE + R \qquad [1]$$

Where G is the net flux into the surface, S is the solar flux minus a portion reflected back to space given by the surface albedo, α. $LW{\downarrow}$ is the longwave flux emitted from atmospheric gases and dust. $LW{\uparrow}$ is the longwave flux emitted from the surface. H is the latent heat flux, describing the exchange in energy between the surface and near-surface atmosphere. LE is the latent heat, representing the phase change of water. The last term, R, is the longwave flux emitted from the clouds, referred to as "cloud emission" throughout. R is an independent parameter in the model, calculated in 2-hour intervals.

Because the Phoenix lander was not equipped with a ground temperature sensor, the thermal environment of the site is modelled numerically. This was achieved using the subsurface conduction model of Schörghofer (2020), with physical parameters tuned to the Phoenix site. The model included a 2-layer scheme, where subsurface ice began at 10.4 cm deep, within the range of depths uncovered by the Robotic Arm (Mellon et al., 2009).

The ground and 2 m air temperature are related to the sensible heat flux by

$$H = k^2 c_p u \rho_a f(R_b) \frac{T_g - T_a}{\ln^2\left(\frac{z_a}{z_0}\right)} \qquad [2]$$

where k is the Von Karman constant, c_p is the specific heat capacity of CO_2, u is the wind-speed, $\rho_{a\,\mathrm{is}}$ the density of the air at 2 m, $f(R_b)$ is a thermal stability term, z_0 is the height at which the air temperature is measured, and z_a is the surface roughness.

The air temperature is plotted in time steps of 120 s and compared to the data acquired from the MET instrument. If the modelled temperature and MET temperature are equal, R is set to zero over the entire run of the model. If the temperatures differ, R is varied on 2-hour intervals to match the modelled temperature to the MET data. By doing this for each sol of the mission, the amount of cloud emission in the energy balance necessary to match the MET

temperature data is found, creating a record of clouds throughout the mission.

It is important to note that, while the temperature is modelled over a full diurnal cycle, cloud emission is only considered between 22:00 to 10:00 local true solar time (LTST). During the day, the near-surface layer is super-adiabatic (Smith et al., 2006), meaning convection is influential when determining the temperature. This can be seen in the turbulent daytime temperatures in Figure 1. However, at nighttime, the atmosphere becomes much more stable. Because the daytime convection is not included in the model, isolating the cloud emission from the energy balance is not possible. As such, we limit the scope of this work to the time of day when radiation is the dominant heat transporting mechanism.

Results:

The modelled temperature, energy balance, and cloud emission for sols 9-10, 64-65, and 137-138 are shown in Figure 1. These sols were chosen as they represent a range in the values of *R* that were found throughout the mission. The rightmost panels show the buildup and decay of the cloud emission through the night, representing the formation and dissipation of clouds. On sol 9-10, the modelled temperature fit the MET temperature well, so no cloud emission was needed in the surface energy balance, representing a day with no clouds. On sol 64-65, up to 5 W m^{-2} emitted from clouds is needed to ensure the modelled temperature fits the MET data. On sol 137-138, the highest value of *R* is 10 W m^{-2}.

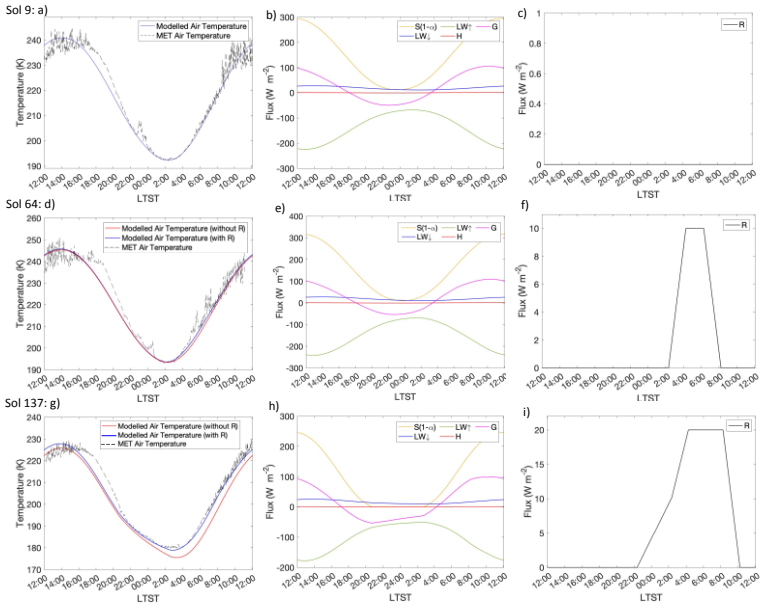

Figure 1: *2 m air temperature on (a) sols 9-10, (d) sols 64-65, and (c) sols 137-138. The red line represents the temperature when the model is run with R = 0 over the entire run. The blue line represents the temperature with R values from the corresponding righthand panel (c, f, and i). The dashed gray line is the MET temperature. The center panels (b, e, and h) show the remaining terms in Equation 1.*

We complete this analysis for each sol to investigate cloud emission as a function of time over the entire mission, as shown in Figure 2. At the beginning of the mission, cloud emission is sparse, with low values around 5 W m^{-2}. Toward the middle of the mission, from sols 55 to 80, the cloud emission reaches a minimum. There are several sols with no emission whatsoever, indicating no clouds formed throughout the night. During this time, on the sols where clouds are present, the cloud emission is shown to begin around 02:00 LTST, corresponding with the coldest point of the night. This minimum in cloud emission coincides with the time after summer solstice when the nighttime atmospheric temperature is highest. From sol 90 until the end of the mission, the cloud emission reaches its highest values. Most sols show the presence of clouds, with values up to and surpassing 20 W m^{-2}. Throughout the entire mission, the cloud emission gets larger throughout the night, with the highest flux in the energy balance from the clouds occurring between 02:00 and 06:00 LTST.

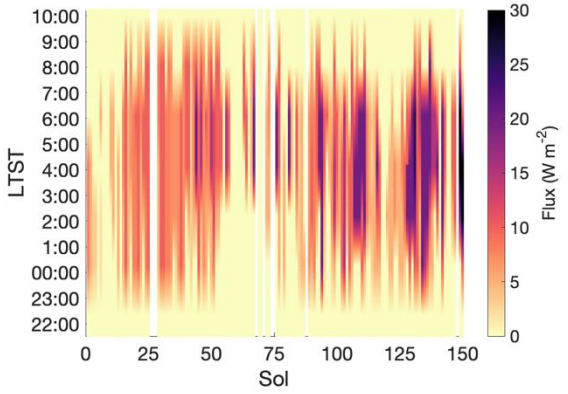

Figure 2: *A near-continuous record of nighttime clouds is built by analyzing the cloud emission as a function of time throughout the entire Phoenix mission.*

As clouds emit longwave flux toward the surface during the nighttime, there is an increase in the surface and near-surface temperature. We investigate this temperature change by taking the difference between the temperature model when it is run with and without *R* introduced, shown in Figure 3. The clouds typically induced a small warming effect, between 1 – 4 K. Toward the end of the mission, when the cloud emission was highest, the temperature was up to 8 K warmer than it would have been without the presence of clouds.

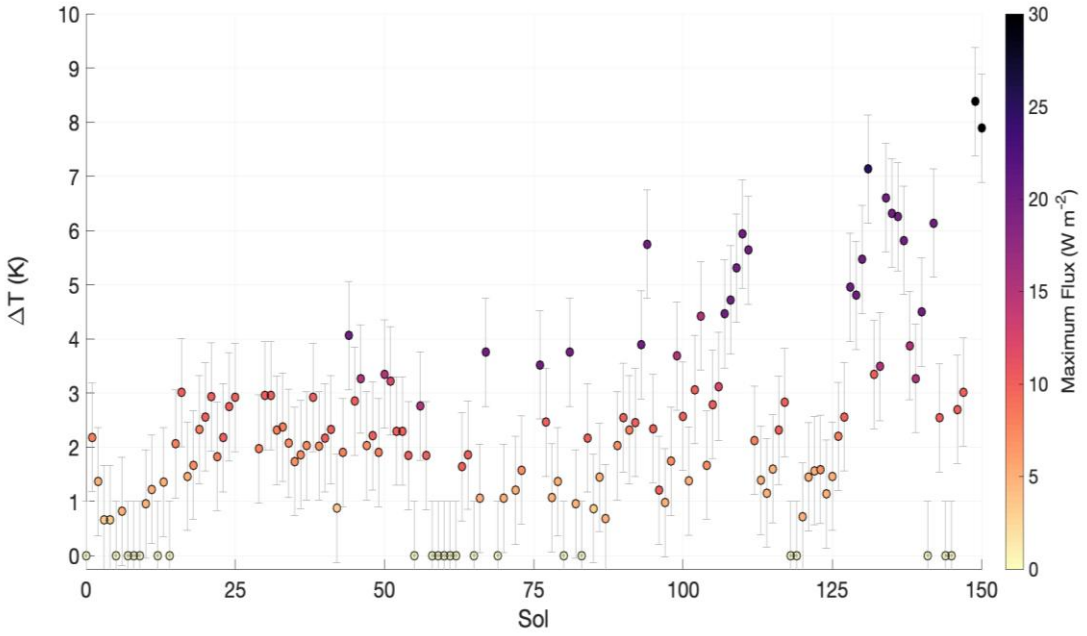

Figure 3: *The maximum change in the 2 m air temperature from 22:00 to 10:00 LTST due to the longwave flux emitted from clouds above the Phoenix lander. Errors bars represent an uncertainty of ± 1K, consistent with uncertainty from the MET temperature sensor.*

Discussion:

This work suggests clouds were present at the Phoenix landing site before they were detected by the SSI or lidar. The lidar was precluded from nighttime operation until sol 38, where water ice-fog was observed. Water-ice retrievals from the Thermal Emission Spectrometer on Mars Global Surveyor in the late northern spring show the presence of clouds in northern polar region of Mars (Tamparri et al. 2008). Sporadic water-ice clouds were detected in the period between 12:30 and 14:30 LTST. The presence of afternoon clouds suggests clouds could have formed over the Phoenix site during the coolest part of the night. Additionally, Moores et al. (2010) note an increase in the optical depth at the beginning of the mission, where they noted this increase could be due to dust and not necessarily indicate water-ice clouds. However, the increase in optical depth in the beginning of the mission and drop in optical depth near the middle of the mission shown in Moores et al. (2010) is similar to the trend in cloud emission seen in Figure 2.

Each year, around L_s = 120° at 60°N, an annular cloud forms, seen in images taken from the Mars Reconnaissance Orbiter and Mars Express (Sánchez-Lavega et al. 2018). During the year the Phoenix mission occurred, a double cyclone produced cloud phenomena, beginning at L_s = 118° (Sánchez-Lavega et al. 2018). The increase in cloud emission around sol 90 in Figure 2 coincides with the formation of the annular cloud, indicating the increase in cloud emission is due to the annular cloud reaching the landing site. Additionally, Sánchez-Lavega et al. 2018 note that years in which there was high coverage of the annular cloud show a rapid sol-tol-sol evolution of the cloud. This agrees with Figure 3, where the temperature change varies from each sol.

The lidar ran frequently overnight after sol 60, showing the ice-water content and water-ice optical depth of the clouds throughout the latter half the mission (Dickinson et al. 2010). We investigated the properties of the water-ice cloud by analyzing the cloud emission as a function of water-ice optical depth retrieved from the lidar (Figure 4). We see that optically

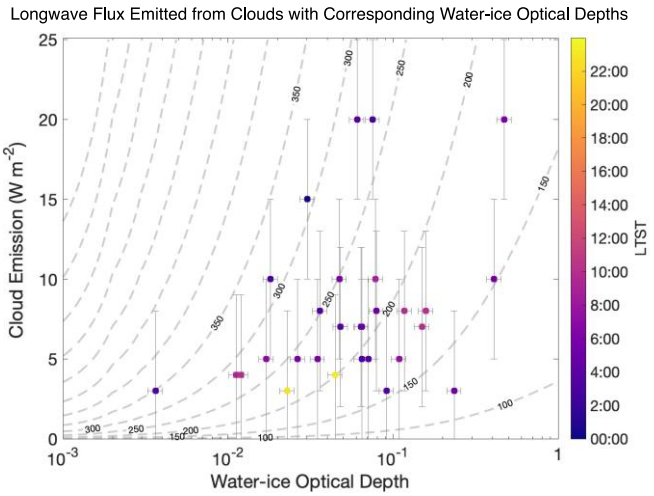

Figure 4: *Cloud emission as a function of water-ice optical depth values measured with the lidar. Con-*

tour lines represent the temperature of the cloud. Horizontal error bars represent the uncertainty in the lidar measurements of ±10%, *cited in Dickinson et al. (2010), The vertical error bars are given as* ± *5 W* m^{-2}, *consistent with the uncertainty in the MET instrument.*

thicker clouds radiate more longwave flux toward the
surface, with an increase in optical depth throughout the night. On some occasions, clouds with different optical depths have similar values of emission. Terrestrial studies have shown that a cloud composed of aggregates emits more thermal radiation than that made of spherical particles (Wendish et al. 2007). A more thorough understanding of cloud microphysics is needed to explain the thermal emission from water-ice clouds.

Conclusions

A record of water-ice cloud throughout the Phoenix mission was built by modelling the 2 m air temperature collected by the MET temperature sensor. The amount of cloud emission was found over the mission, filling in temporal gaps left by the lidar and SSI.

A diurnal cycle was seen, where the cloud emission increased throughout the night, typically reaching a peak between 02:00 and 06:00 LTST, and dissipating into the morning. In addition, as a seasonal cycle was observed, where sporadic clouds were seen in the beginning of the mission and reached a minimum by the middle of the mission. From sol 90 onward, the highest amount of cloud emission occurred, reaching values upwards of 20 W m^{-2}. This induced a warming effect at the surface, raising the 2 m air temperature, usually by 1 – 3 K.

This analysis can be expanded to other regions of Mars to build cloud records by analyzing the energy balance. This would build a cloud record at other locations where temporal gaps may exist. In addition, analyzing the cloud emission as a function of water-ice optical depth may provide a valuable comparison between equatorial and polar clouds.

Acknowledgements

This work was funded in part by the Natural Sciences and Engineering Research Council of Canada (NSERC) Technologies for Exo-planetary Science (TEPS) Collaborative Research and Training Experience (CREATE) program. The authors wish to thank Jim Whiteway for providing the optical depth data obtained from the lidar used in the discussion of this analysis.

References

Cooper, B.A., de la Torre Juárez, M., Mischna, M. et al. 2021., Journal of Geophysical Research: Planets, 126, e2020JE006737, doi: https://doi.org/10.1029/2020JE006737

Dickinson, C., Whiteway, J. A., Komguem, L., Moores, J. E., & Lemmon, M. T. 2010, Geophysical Research Letters, 37, L18203, doi: https://doi.org/10.1029/2010GL044317

Martínez, G. M., Renn´o, N., Fischer, E., et al. 2014, Journal of Geophysical Research: Planets, 119, 1822, doi: https://doi.org/10.1002/2014JE004618

Mellon, M. T., Arvidson, R. E., Sizemore, H. G., et al. 2009, Journal of Geophysical Research: Planets, 114, E00E07, doi: https://doi.org/10.1029/2009JE003417

Moores, J. E., Lemmon, M. T., Smith, P. H., Komguem, L., & Whiteway, J. A. 2010, Journal of Geophysical Research: Planets, 115, E00E08, doi: https://doi.org/10.1029/2009JE003409

Sánchez-Lavega, A., Garro, A., del Río-Gaztelurrutia, T., et al. 2018, Journal of Geophysical Research: Planets, 123, 3020– 3034, doi: https://doi.org/10.1029/2018JE005740

Schorghofer, N. 2020, Planetary-Code-Collection: Thermal and Ice Evolution Models for Planetary Surfaces v1.1.7, GitHub. doi:10.5281/zenodo.594268 https://github.com/nschorgh/ Planetary-Code-Collection/

Smith, M. D., Wolff, M. J., Spanovich, N., et al. 2006, Journal of Geophysical Research: Planets, 111, E12S13, https://doi.org/doi:10.1029/2006JE002770

Tamppari, L.K., Smith, M.D., Bass, D.S., et al. 2008, Planetary and Space Science, 56, 227-245, doi: https://doi.org/10.1016/j.pss.2007.08.011

Taylor, P. A., Catling, D. C., Daly, M., et al. 2008, Journal of Geophysical Research: Planets, 113, E00A10, doi: https://doi.org/10.1029/2007JE003015

Whiteway, J. A., Komguem, L., Dickinson, C., et al. 2009, Science, 325, 68, doi: https://doi.org/10.1126/science.1172344

Wilson, R. J., Neumann, G. A., & Smith, M. D. 2007, Geophysical Research Letters, 34, L02710, doi: https://doi.org/10.1029/2006GL027976

Wendisch, M., Yang, P., Pilewskie, P. 2007, Journal of Geophysical Research, 112, D08201, doi: https://doi.org/10.1029/2006JD007899